Nucleation-type magnetization reversal by spin-polarized current in perpendicularly magnetized FePt layers

Takeshi Seki,* Seiji Mitani, and Koki Takanashi
Institute for Materials Research, Tohoku University, 2-1-1 Katahira, Aoba-ku, Sendai 980-8577, Japan
(Received 18 October 2007; revised manuscript received 14 March 2008; published 10 June 2008)

The magnetic field dependence of current-induced magnetization reversal was investigated for current-perpendicular-to-plane giant magnetoresistance pillars with perpendicularly magnetized FePt layers. Current-induced magnetization reversal under the tilted external magnetic field showed that a reversed domain is nucleated by spin-transfer torque and then propagates to complete magnetization reversal, although the formation of a multiple-domain state is not observed by static measurement. This nucleation-type current-induced magnetization reversal is characteristic of a system having large magnetic anisotropy and a small number of pinning sites for the domain wall, and explains the large magnetic field dependence of the critical current density for magnetization reversal (J_c). As the magnetic anisotropy of the FePt free layer is reduced, the magnetic field dependence of J_c becomes close to the values theoretically calculated for the coherent rotation mode, implying that the mode of the current-induced magnetization reversal changes from the nucleation of a reversed domain to the rotation of magnetization.

DOI: 10.1103/PhysRevB.77.214414 PACS number(s): 85.75.−d, 72.25.Ba, 75.47.De, 75.60.Jk

I. INTRODUCTION

Theoretical predictions[1,2] followed by experimental demonstrations[3–15] of magnetization precession and reversal by spin-polarized current are generally based on the physics of spin-transfer torque. When spin-polarized current passes through a nanometer-sized magnet, the spin angular momentum of the electrons is transferred to the local spins of the magnet and the spin angular momentum transfer gives rise to the magnetization excitation. Therefore, in a multilayered structure consisting of a ferromagnetic free layer and a spin-polarizer separated by a nonmagnetic layer or an insulator, the magnetization direction of the free layer can be controlled by passing spin-polarized current through the multilayered structure. This finding has opened up a way for the further advances in spin-electronics.

Although most of the experimental demonstrations have been performed in current-perpendicular-to-plane giant magnetoresistance (CPP-GMR) pillars or magnetic tunnel junctions consisting entirely of in-plane magnetized layers, only a few studies of current-induced magnetization reversal in perpendicular magnetization configurations have been reported to date,[16–18] in which both the free layer and the spin-polarizer are magnetized perpendicularly to the film plane. In one of these studies,[17] the current-induced magnetization reversal from an antiparallel (AP) to a parallel (P) alignment was observed for CPP-GMR pillars with perpendicularly magnetized $L1_0$-FePt layers while a large applied magnetic field close to the coercivity (H_c) of the free layer was required due to the large uniaxial magnetic anisotropy (K_u) of 5×10^7 erg/cm^3. In addition, the critical current densities for the magnetization reversal (J_c) showed anomalously large magnetic field dependence, which is not explained by the theoretical calculation assuming the coherent magnetization rotation. Ravelosona *et al.*[19] reported the creation of a domain wall due to spin-transfer torque in similar perpendicularly magnetized CPP-GMR pillars with Co/Ni multilayers. Their finding is physically important and suggests that the nucleation of reversed domains plays a key role in the current-induced magnetization reversal for perpendicular magnetization as well as magnetization reversal by magnetic field. However, its detailed mechanism remains to be elusive, *e.g.,* the effect of the nucleation of reversed domains on J_c, and the relationship between the magnetization reversal mode and the magnitude of K_u.

The present paper reports the magnetic field dependence of current-induced magnetization reversal for CPP-GMR pillars with perpendicularly magnetized $L1_0$-FePt layers, in which the degree of chemical order and, consequently, the magnitude of K_u are varied by annealing the $L1_0$-FePt layer at different temperatures. The dependence of H_c and J_c on the angle of the applied magnetic field is analyzed, and the mode of magnetization reversal induced by spin-polarized current is discussed for perpendicularly magnetized FePt layers.

II. EXPERIMENTAL PROCEDURE

Thin films were prepared on MgO (001) single crystal substrates using an ultrahigh vacuum magnetron sputtering system with separate targets of Fe, Pt, and Au. Base pressure was below 2×10^{-9} Torr, and high purity argon was flown during sputtering. A typical deposition rate was 0.01 nm/sec. The stacking structure for microfabricated samples is MgO subs./Fe(1)/Au(100)/$L1_0$-FePt(20)/Fe(1)/Au(5)/$L1_0$-FePt(4)/Au(25)/Pt(100) (in nanometers). All the layers except the $L1_0$-FePt layers were deposited at room temperature (RT), and the $L1_0$-FePt layers were deposited at 300 °C. To promote the $L1_0$ ordering, the $L1_0$-FePt layers were subsequently annealed for 15 minutes. The annealing temperature (T_{ann}) for the top 4 nm-thick FePt layer was varied in the range from 400 °C to 500 °C. On the other hand, T_{ann} for the bottom 20 nm-thick FePt layer was fixed at 500 °C. The composition of the FePt layers was $Fe_{43}Pt_{57}$. The 1 nm-thick Fe seed and 100 nm-thick Au buffer layers are required for the epitaxial growth of the bottom 20 nm-thick $L1_0$-FePt

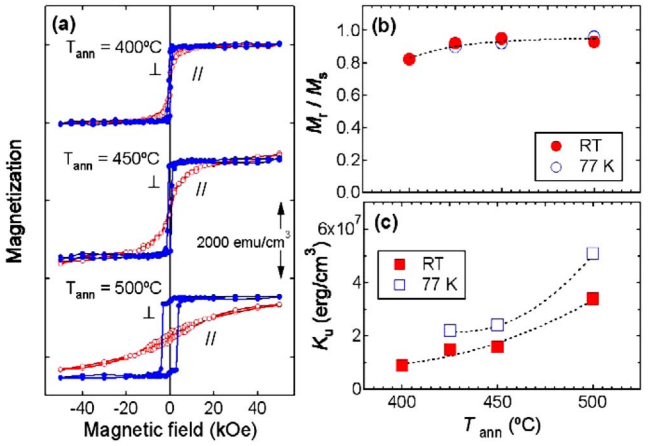

FIG. 1. (Color online) (a) Magnetization curves for the 4 nm-thick FePt thin films annealed at 400 °C, 450 °C and 500 °C, where solid and open circles are the results with fields applied perpendicular and parallel to the film plane, respectively. (The magnetization curves for 500 °C are reproduced from Ref. 17) (b) The ratio of remanent magnetization to saturation magnetization (M_r/M_s) and (c) the uniaxial magnetic anisotropy (K_u) as a function of annealing temperature (T_{ann}). The solid and open marks represent the data obtained at RT and 77 K, respectively.

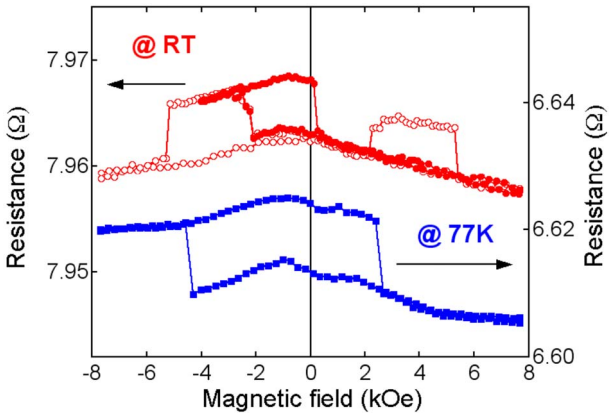

FIG. 2. (Color online) (a) MR curves for the CPP-GMR pillar with the 4 nm-thick FePt layer annealed at 450 °C. The measurement temperatures are RT (circles and left-hand axis) and 77 K (squares and right-hand axis). The open and solid marks represent the full and minor MR curves, respectively.

layer. The 1 nm-thick Fe intermediate layer plays a role to maintain the (001) orientation of the 5 nm-thick Au layer and the top FePt layer. The epitaxial growth and the formation of the $L1_0$ ordered structure were confirmed by x-ray diffraction. The preferential crystallographic orientation is the [001] direction.

The samples were fabricated into a CPP geometry using electron beam lithography and Ar ion etching. The microfabrication process used in the present study is as follows: The thin film was first patterned into a bottom lead shape. Then, the lead-shaped thin film was etched into the Au buffer layer using a negative resist mask of a pillar shape. The pillar size was 0.1×0.2 μm^2, and both the top and bottom FePt layers were microfabricated into the pillar shape. After patterning, an Al-O insulating layer with a thickness of 100 nm was deposited and the resist mask was lifted off. Finally, a top lead of Pt was formed using a conventional lift-off technique. In addition to the microfabricated samples, thin films of MgO(001)subs./Fe(1 nm)/Au(40 nm)/$L1_0$-FePt (4 nm) were prepared to investigate the change of the magnetic properties with T_{ann}.

Transport properties were measured using a dc four-probe method. A small sensing current of 0.5 mA was used for the resistance measurement. Current-induced magnetization reversal was characterized using a current pulse sequence with a pulse duration of 0.1 msec.[20] The sign of the direction of electrical current flowing from the thicker FePt layer to the thinner FePt layer is defined as positive. Magnetic properties were measured with a superconducting quantum interference device magnetometer.

III. MAGNETIC PROPERTIES OF FEPT LAYERS

Figure 1(a) shows magnetization curves for the 4 nm-thick $L1_0$-FePt layers annealed at different temperatures (T_{ann}=400 °C, 450 °C, and 500 °C). The solid and open marks represent the results with fields applied perpendicular and parallel to the film plane, respectively. Although the easy magnetization axes for all the films are perpendicular to the film plane, the saturation field of the magnetization in the in-plane direction increases with increasing T_{ann}, and the maximum magnetic field of 50 kOe is not sufficient to saturate the magnetization for T_{ann}=500 °C. The ratio of the remanent magnetization to the saturation magnetization (M_r/M_s) and K_u as a function of T_{ann} are summarized in Figs. 1(b) and 1(c), respectively. The solid and open marks are the data at RT and 77 K, respectively. The high M_r/M_s for $T_{ann} \geq 400$ °C indicates that T_{ann}=400 °C is high enough to achieve good squareness of the magnetization curve, which is indispensable to achieve the bistable state at zero magnetic field in magnetoresistance (MR) curves. The value of K_u was obtained from the effective magnetic anisotropy energy (K_u^{eff}), which was evaluated from the enclosed area between the perpendicular and in-plane magnetization curves and the correction of the shape anisotropy energy ($K_d = -2\pi M_s^2$), that is, $K_u = K_u^{eff} + 2\pi M_s^2$. K_u gradually increases with T_{ann} because high T_{ann} promotes the $L1_0$ ordering of the FePt layer. These results show that the magnitude of K_u is controlled by changing T_{ann} while the high M_r/M_s is maintained.

IV. MAGNETORESISTANCE AND CURRENT-INDUCED MAGNETIZATION REVERSAL

MR curves for T_{ann}=450 °C measured at RT (circles) and 77 K (squares) are shown in Fig. 2. The open and closed marks represent the full and minor MR curves, respectively. The magnetic field was applied perpendicularly to the film plane. Resistance changes are clearly observed at both temperatures; the high and low resistance values are attributable to the AP and P alignments of the two $L1_0$-FePt layers, respectively. Annealing of the 20 nm-thick bottom $L1_0$-FePt layer at 500 °C resulted in higher K_u than that of the 4 nm-

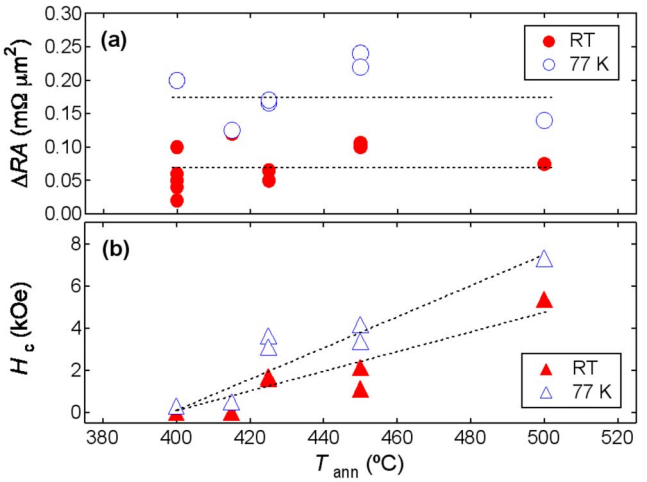

FIG. 3. (Color online) (a) Resistance – area product (ΔRA) and (b) coercivity (H_c) as a function of annealing temperature (T_{ann}). The solid and open marks represent the results at RT and 77 K, respectively. The dashed lines are guides for the eyes.

thick top $L1_0$-FePt layer, which was annealed at 450 °C . Therefore, the magnetization of the 4 nm-thick $L1_0$-FePt layer is more easily switched by magnetic field than that of the 20 nm-thick $L1_0$-FePt layer. The MR curves show the backgrounds of the resistance which decrease with increasing the magnetic field. Those backgrounds may result from the existence of some components with the magnetization tilted from the perpendicular direction, which is due to the damaged area induced by microfabrication,[21] and the tilted magnetization may be aligned by the perpendicular magnetic field. Since a clear hysteresis loop showing stable AP and P states is obtained in the minor MR curve, the MR curve for T_{ann}=450 °C is suitable for the static measurement of the current-induced magnetization reversal. Figures 3(a) and 3(b) summarize the product of the resistance change and the pillar area (ΔRA) and H_c, respectively, for the minor MR curves as a function of T_{ann}. Dashed lines are guides for the eyes. ΔRA does not significantly depend on T_{ann}. H_c increases with T_{ann}, which results from the increase in K_u with T_{ann}. For T_{ann}=400 °C, H_c is smaller than 0.5 kOe and no clear hysteresis loop is observed in the minor MR curve. The low squareness of the minor MR curve for T_{ann}=400 °C is inconsistent with the magnetization curve for T_{ann}=400 °C showing high M_r/M_s. A possible explanation for this inconsistency is that a part of the pillar has K_u lower than that of the unpatterned thin film because of the microfabrication damage[21] and it starts the magnetization reversal at a small magnetic field, leading to the degradation of squareness of the MR curves for the CPP-GMR pillar.

Figure 4 shows resistance (R) versus current pulse (I_P) for T_{ann}=450 °C at the applied magnetic field (H_{appl}) of (a) −3.2 kOe, (b) −2.6 kOe, (c) 0 Oe, (d) 1 kOe, and (e) 1.9 kOe. The measurement was performed at 77 K, and the sample resistance was measured using a sensing current of 0.5 mA after applying a current pulse. The corresponding minor MR curve is shown in Fig. 2, and the direction of H_{appl} is the same as that in the MR curve. The open circles are the results of the measurements starting from the P state and the

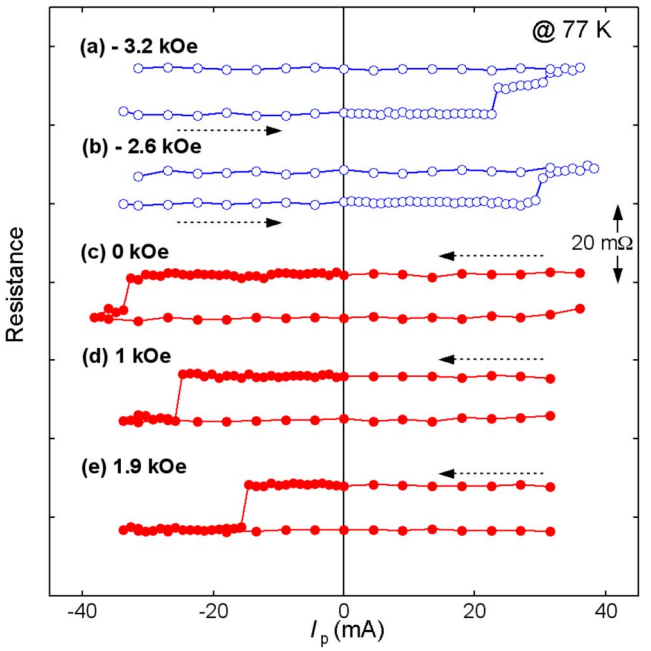

FIG. 4. (Color online) Resistance (R)-current pulse (I_P) curves for the CPP-GMR pillar with the 4 nm-thick FePt layer annealed at 450 °C. The R-I_P curves were obtained at the applied magnetic field (H_{appl}) of (a) −3.2 kOe, (b) −2.6 kOe, (c) 0 Oe, (d) 1 kOe, and (e) 1.9 kOe. The measurement was performed at 77 K, and the sample resistance was measured using the sensing current of 0.5 mA after applying the current pulse. The open circles represent the results of the measurements starting from the parallel state and the negative current direction. The solid circles are the results of the measurements starting from the antiparallel state and the positive current direction.

negative current direction, whereas the solid circles are obtained starting from the AP state and the positive current direction. At the positive H_{appl}, a resistance drop resulting from the change of magnetization alignment from AP to P is observed only in the negative current region. With decreasing H_{appl}, the critical current for the magnetization reversal (I_c) gradually increases. At negative H_{appl}, on the other hand, a resistance jump appears in the positive current region. Although the magnitude of ΔR for the positive H_{appl}, which is almost equal to that obtained in the MR curve, indicates full magnetization reversal, the smaller ΔR for H_{appl}=−2.6 kOe means that the intermediate state (IS) of resistance appears during magnetization reversal. The IS corresponds to the formation of a multiple domain.[19] The previous papers of Refs. 16 and 19 reported that the IS states were observed in a low magnetic field region. In the present case, however, the IS states appear at large H_{appl}. This may result from the narrow domain wall width of the present FePt layer due to its high K_u, which leads to a stable multiple-domain state. With increasing H_{appl} to −3.2 kOe, the full magnetization reversal from P to AP occurs through the formation of a multiple-domain state.

The phase diagram of I_p as a function of H_{appl} is shown in Fig. 5. The solid circles, open squares, and solid squares represent the values of I_c for the transition from AP to P, from P to IS, and from IS to AP, respectively. Calculated

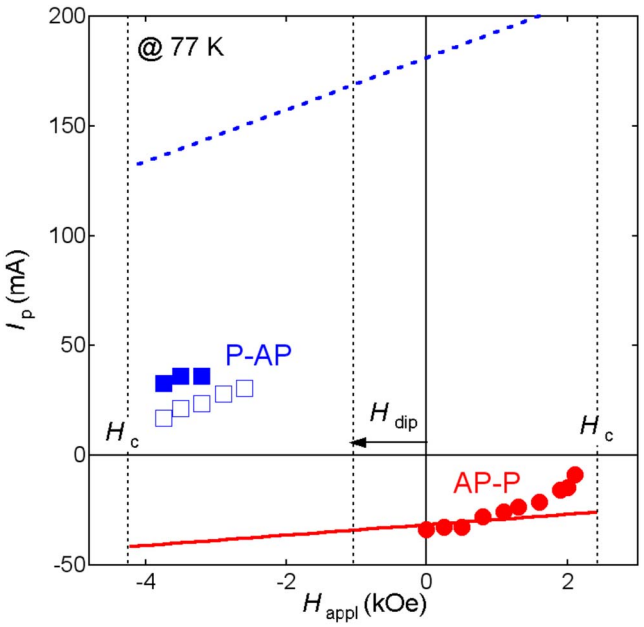

FIG. 5. (Color online) Static phase diagram of current pulse for the magnetization reversal (I_P) versus applied magnetic field (H_{appl}) at 77 K for the CPP-GMR pillar with the 4 nm-thick FePt layer annealed at 450 °C. The solid circles, open squares, and solid squares represent the current for magnetization reversal (I_c) for the transition from AP to P, from P to IS, and from IS to AP, respectively. The calculated results are also shown as solid (from AP to P) and broken lines (from P to AP).

results are also shown as solid (from AP to P) and broken lines (from P to AP). The present measurement uses the current pulse sequence with the pulse duration of 0.1 msec which is too long to eliminate the effect of the thermal activation. According to the spin-transfer theory taking into account thermal activation, which assumes that magnetization reversal occurs through the coherent rotation mode, I_c is described as[22–24]

$$I_c = I_{c0}[1 - (k_B T/\Delta E)\mathrm{In}(\tau_p/\tau_0)], \quad (1)$$

where k_B is the Boltzmann constant, T is the measurement temperature, ΔE is the energy barrier, τ_p is the current pulse width, and τ_0 is the inverse of the attempt frequency. I_{c0} is the intrinsic I_c without thermal activation and is described as[1]

$$I_{c0} = \alpha e \gamma V M_s H_{\mathrm{eff}}/\mu_B g(\theta), \quad (2)$$

where α is the damping parameter, e is the elementary charge, γ is the gyromagnetic ratio, V is the magnetic volume, and μ_B is the Bohr magneton. $g(\theta)$ is the spin-transfer efficiency, which is related to the spin-polarization factor (P) and is a function of the relative angle (θ) between the two ferromagnetic layers. H_{eff} is the effective magnetic field including H_{appl}, anisotropy field (H_a), dipole coupling field (H_{dip}), and demagnetizing field (H_d). H_a is $2K_u/M_s$. H_{dip} is an effective field resulting from a stray field around the edge of the pillar and the stray field due to the interface roughness. In the case of perpendicular magnetization, H_d is given by $-4\pi M_s$ because of its negative shape anisotropy. ΔE is expressed as

$$\Delta E = K_u^{\mathrm{eff}} V\left(1 \pm \frac{H_{\mathrm{appl}}}{H_a^{\mathrm{eff}}}\right)^2 = K_u^{\mathrm{eff}} V\left(1 \pm \frac{H_{\mathrm{appl}} M_s}{2K_u^{\mathrm{eff}}}\right)^2, \quad (3)$$

where $H_a^{\mathrm{eff}} = H_a - H_d$ and the upper (lower) sign labels ΔE for the AP-P (P-AP) transition. In the present study, the parameters of $K_u = 2 \times 10^7$ erg/cm^3, $M_s = 1350$ emu/cm^3, and $H_{\mathrm{dip}} = -1.1$ kOe are experimentally obtained. $\alpha = 0.05$ and $T = 77$ K are used. P is assumed to be 0.4 on the basis of a previous study of current-induced magnetization reversal for in-plane magnetized FePt layers.[25] The calculated values for AP-P are close to the experimental ones whereas those for P-AP are quite larger than the experimental ones. The reason for the smaller experimental values of P-AP than the calculation is not clear at present. It is possibly due to a large thermal effect induced by the applied current. The observation of P-AP requires the larger applied current and the larger H_{appl} compared to that of AP-P, in which a reversed domain might thermally nucleate due to the sample heating by current. Another possible reason is that the $g(\theta)$ function[1] used in the present study leads to a large asymmetry of calculated I_c between the transitions of AP-P and P-AP. It was reported that the different $g(\theta)$ function enhances the spin-transfer efficiency for P-AP and reduces its asymmetry of the calculated I_c.[26] Therefore, such a $g(\theta)$ function may provide a better fit for the P-AP transition.

The multiple-domain state is stable during the transition from P to AP, implying that the process of magnetization reversal of P-AP is particularly complicated. On the other hand, no multiple-domain state is observed for AP-P, and furthermore the calculation for AP-P is in relatively good agreement with the experimental results, especially in a low magnetic field region around $H_{\mathrm{appl}} = 0$. With increasing H_{appl}, however, the experimental results gradually deviate from the calculated results. The following section focuses on the magnetic field dependence of I_c for the transition from AP to P, and its magnetization reversal mode is discussed.

V. ANGULAR DEPENDENCE OF MAGNETIZATION REVERSAL

The dependence of the MR curves on the angle of the magnetic field is first investigated to understand the behavior of field-induced magnetization reversal. Figure 6(a) shows MR curves with the magnetic field tilted with respect to the surface normal. The shape of MR curves obviously changes with increasing the tilt angle (ϕ). For the transition from P to AP, a multiple domain appears with increasing ϕ, implying the complicated magnetization reversal process for P-AP as in the case of current-induced magnetization reversal. For AP-P, on the other hand, H_c gradually decreases and no stable multiple-domain state is observed. H_c normalized by H_c at $\phi = 0$ and ΔR in the MR curves as a function of ϕ are shown in Figs. 6(b) and 6(c), respectively, where H_c is the switching field from AP to P. The angular dependence of H_c does not follow the $1/\cos\phi$ law of the domain wall motion, but rather shows a downward curvature. Since ΔR does not

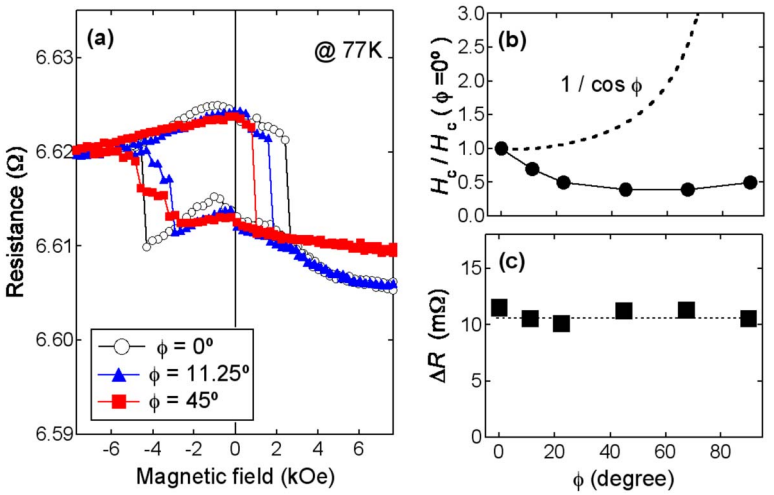

FIG. 6. (Color online) (a) MR curves at 77 K for the CPP-GMR pillar with the 4 nm-thick FePt layer annealed at 450 °C. The MR curves were measured under the magnetic field tilted with respect to the surface normal. The circles, triangles, and squares represent MR measured at the tilt angles (ϕ) of 0°, 11.25°, and 45°, respectively. (b) Coercivity (H_c) normalized by H_c at ϕ=0 and (c) resistance change (ΔR) at 77 K as a function of ϕ.

depend strongly on ϕ, the relative angle between the magnetization vectors for the two $L1_0$-FePt layers remains constant even under the tilted external magnetic field. From the result of the angular dependence of H_c, the magnetization reversal mode by external magnetic field is discussed. In the case of coherent rotation mode, H_c is given by

$$H_c = H_a^{\text{eff}} = \frac{2K_u^{\text{eff}}}{M_s}. \tag{4}$$

If the coherent rotation is dominant for the present FePt layer, large H_c=12.5 kOe should be obtained due to the high K_u, which is much larger than the experimental H_c. Instead of coherent rotation, one possible magnetization reversal process in the present CPP-GMR pillar is that a reversed domain nucleate and the domain wall subsequently propagate. The nucleation of a reversed domain means that a multiple-domain state once appears. If the multiple-domain state is stable and the domain walls are pinned by a pinning potential, the angular dependence of H_c should show the tendency of $1/\cos\phi$ because the pressure on the domain walls is a function of $1/\cos\phi$. However, the fact that the angular dependence of H_c does not follow the $1/\cos\phi$ law indicates that the domain wall moves without significant pinning. Consequently, the field-induced magnetization reversal in the present FePt layer is a nucleation-type. In other words, H_c in the MR curve is mainly determined by the nucleation field (H_n).

Next, the magnetic field dependence of current-induced magnetization reversal with the tilted magnetic field is discussed. Figure 7 shows I_c for the AP-P transition as a function of ϕ at H_{appl}=0.25 kOe (circles), 0.8 kOe (triangles), and 1.3 kOe (squares). For H_{appl}=0.25 kOe, I_c remains almost constant regardless of ϕ. With increasing H_{appl} to 0.8 kOe, the angular dependence of I_c shows a convex downward curve. In the case of H_{appl}=1.3 kOe, the current-induced magnetization reversal is observed only at small ϕ.

Theoretical and experimental studies[27,28] have shown that a spin-polarized current excites magnetization precession, and when the magnitude of magnetization precession overcomes the barrier of the potential energy, magnetization reversal occurs. Applying external magnetic field corresponds to changing the height of the energy barrier ($\Delta\varepsilon$) as schematically illustrated in Fig. 8(a). Therefore, the magnitude of I_c is considered to be equal to the energy for overcoming $\Delta\varepsilon$ [Fig. 8(b)], where it is assumed that $g(\theta)$ does not depend on the angle of external magnetic field because ΔR for the present sample does not show the angular dependence. When external magnetic field is applied in the direction of ϕ, the potential energy (ε) for the magnetization pointing at θ is expressed as

$$\varepsilon = \frac{1}{2}\sin^2\left(\frac{\theta}{180}\pi\right) - h\cos\left[\left(1 - \frac{\theta+\phi}{180}\right)\pi\right], \tag{5}$$

where ε is the energy normalized by $M_s H_a^{\text{eff}}$, θ is the angle of the magnetization with respect to the direction normal to the film plane, and $h = H_{\text{appl}}/H_a^{\text{eff}}$ for the magnetization rotation. Using Eq. (5), ε as a function of θ is obtained for different ϕ,

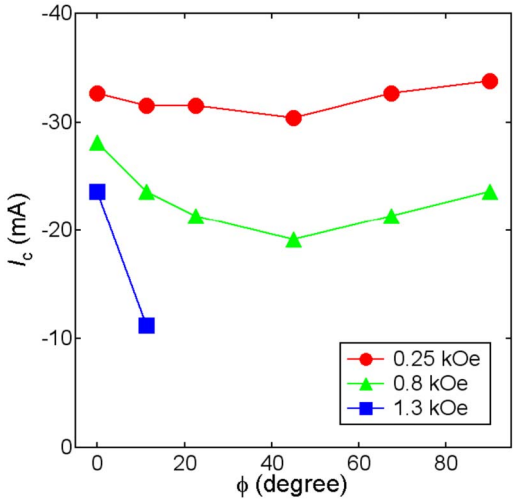

FIG. 7. (Color online) Critical current for the magnetization reversal (I_c) as a function of the tilt angle of external magnetic field (ϕ) for the CPP-GMR pillar with the 4 nm-thick FePt layer annealed at 450 °C. The circles, triangles, and squares represent the data obtained at the magnetic field of 0.25, 0.8, and 1.3 kOe, respectively.

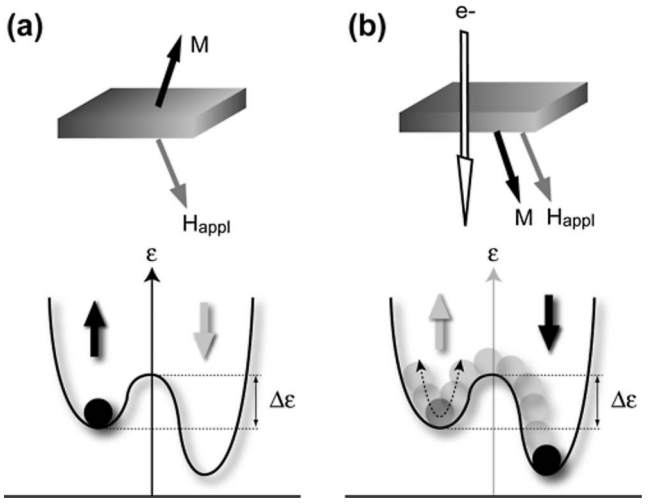

FIG. 8. Schematic of the potential energy for magnetization reversal under the external magnetic field (a) without and (b) with applying the current.

$\Delta\varepsilon$ from the local minimum to the top of the potential barrier is calculated for each ϕ, which corresponds to the energy barrier height for the magnetization reversal.

Figure 9 compares $\Delta\varepsilon$ normalized by $\Delta\varepsilon$ at $\phi=0$ with normalized I_c. The open circles, triangles, and squares in Fig. 9(a) are the normalized I_c for $H_{\text{appl}}=0.25$, 0.8, and 1.3 kOe, respectively. The angular dependence of normalized $\Delta\varepsilon$ is shown in Fig. 9(b) for $h=0.02$ (circles), 0.06 (crosses), 0.10 (inverted triangles), 0.24 (triangles), and 0.39 (squares). Using $H_a^{\text{eff}}=12.5$ kOe, the values of h are calculated to be 0.02, 0.06, and 0.10 for $H_{\text{appl}}=0.25$, 0.8, and 1.3 kOe, respectively. Although the change of $\Delta\varepsilon$ for $h=0.02$ agrees relatively well with the normalized I_c for $H_{\text{appl}}=0.25$ kOe, $\Delta\varepsilon$ for $h=0.06$ is not consistent with the results for $H_{\text{appl}}=0.8$ kOe. If $\Delta\varepsilon$ for current-induced magnetization reversal is determined by H_n as in the case of the field-induced magnetization reversal, h

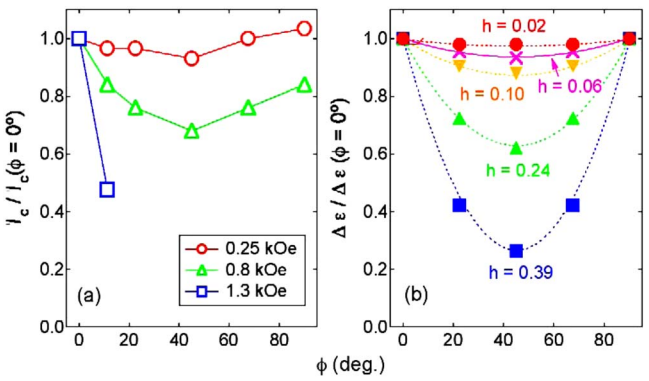

FIG. 9. (Color online) (a) Critical current for the magnetization reversal (I_c) normalized by I_c at the tilt angle of applied magnetic field (ϕ) of 0 and (b) the height of the energy barrier ($\Delta\varepsilon$) normalized by $\Delta\varepsilon$ at $\phi=0$ as a function of ϕ. The open circles, triangles, and squares represent the normalized I_c at the applied magnetic field of 0.25, 0.8, and 1.3 kOe, respectively. The solid marks are the normalized $\Delta\varepsilon$ for $h=0.02$ (circles), 0.06 (crosses), 0.10 (inverted triangles), 0.24 (triangles), and 0.39 (squares), where h is the ratio of the magnetic field to the anisotropy field.

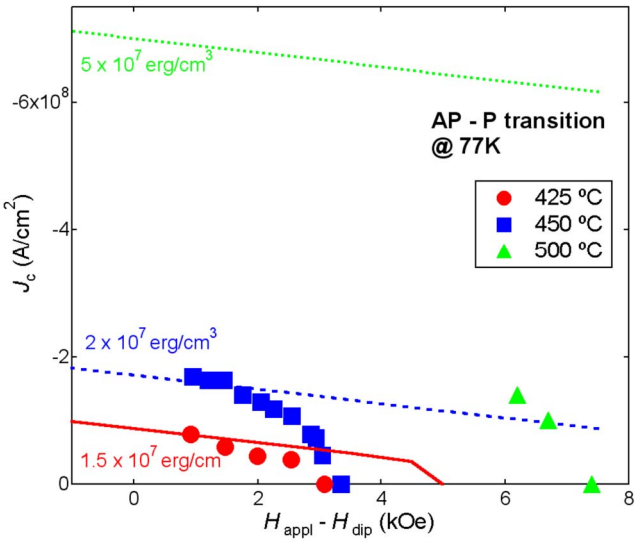

FIG. 10. (Color online) Current density for the magnetization reversal (J_c) from antiparallel to parallel as a function of applied magnetic field (H_{appl}) at 77 K. The 4 nm-thick FePt layers were annealed at 425 °C (circles), 450 °C (squares), and 500 °C (triangles). The solid, broken, and dotted lines represent the calculated results for $K_u=1.5\times10^7$, 2.0×10^7, and 2.0×10^7 erg/cm^3, respectively.

is described as H_{appl}/H_n, where H_n corresponds to H_c-H_{dip}. For $H_{\text{appl}}=0.8$ kOe, h is calculated to be 0.24 using $H_n=3.3$ kOe. Consequently, the variation in $\Delta\varepsilon$ for $h=0.24$ is in agreement with the angular dependence of I_c for $H_{\text{appl}}=0.8$ kOe. These results show that $\Delta\varepsilon$ for the current-induced magnetization reversal in the present $L1_0$-FePt layer is mainly determined by H_n. This nucleation-type magnetization reversal means that the nucleation of a reversed domain by the current is the rate-controlling step. After nucleation, the domain moves smoothly due to the existence of external magnetic field. A conventional material for a free layer such as NiFe or CoFe shows coherent or incoherent rotation due to its thick domain wall, which is comparable to a submicron size of a pillar. However, the thin domain wall in $L1_0$-FePt, typically ~4 nm, enables the appearance of reversed domains during magnetization reversal. In addition, the magnetostatic energy in the perpendicularly magnetized free layer prefers the formation of multiple-domain states. CPP-GMR pillars with Co/Ni multilayers have shown pinning-type current-induced magnetization reversal where the stable multiple-domain state has been observed.[19] Unlike Co/Ni multilayers, nucleation-type current-induced magnetization reversal in the present $L1_0$-FePt layer is the full magnetization reversal through a multiple-domain state even though the multiple-domain is not statically observed in the AP-P transition.

Figure 10 shows the magnetic field dependence of J_c from AP to P for 4 nm-thick FePt layers with different K_u. The free layers in the pillars were annealed at $T_{\text{ann}}=425$ °C (circles), 450 °C (squares), and 500 °C (triangles). The solid, broken, and dotted lines represent the calculated results using $K_u=1.5\times10^7$, 2.0×10^7, and 5.0×10^7 erg/cm^3, respectively. With decreasing T_{ann}, the pillar shows low J_c

due to the reduction of K_u. Although K_u for T_{ann}=450 °C is higher than that for T_{ann}=425 °C, J_c for T_{ann}=450 °C is close to that for T_{ann}=425 °C when H_{appl} increases to H_c. This also indicates the nucleation-type current-induced magnetization reversal where J_c in a high magnetic field is determined by H_n regardless of K_u. With reducing K_u, the experimental data become close to the theoretically calculated magnetic field dependence of J_c, implying that the magnetization reversal mode changes from nucleation to rotation. Recently, an incoherent rotation mode has attracted much attention, and the micromagnetic modeling[29] and the experimental observation[30] have confirmed the existence of incoherent rotation mode during current-induced magnetization reversal even for the in-plane magnetized CPP-GMR pillars. Furthermore, it has been reported that the nonuniform injection of spin-polarized current leads to the domain nucleation during magnetization reversal.[31] The present results show that the nucleation-type magnetization reversal mode is dominant and important for a perpendicularly magnetized free layer with high K_u.

VI. CONCLUSION

The present paper showed the current-induced magnetization reversal for the CPP-GMR pillars with the perpendicularly magnetized $L1_0$-FePt layers. The angular dependence of field- and current-induced magnetization reversal indicated the nucleation-type magnetization reversal mode, and the energy barrier was determined by H_n. A reversed domain was nucleated by spin-transfer torque and then propagated by the external magnetic field, which is a characteristic mode of high magnetic anisotropy materials with small domain wall pinning potential such as the present $L1_0$-FePt layer. The nucleation-type current-induced magnetization reversal is one reason for the observed large magnetic field dependence of J_c. With reducing the magnitude of K_u, J_c decreased and became close to the theoretical calculation on the basis of the coherent rotation mode, implying that the mode of current-induced magnetization reversal changed from nucleation to rotation.

Note added in proof. Recently, a closely related simulation was published.[32]

ACKNOWLEDGMENTS

This work was partially supported by the NEDO Grant program. The structural characterization and the sample fabrication were partly performed at Advanced Research Center of Metallic Glasses, IMR, Tohoku University. The authors would like to acknowledge S. Mangin, H. Imamura, and M. Mizuguchi for helpful discussion and fruitful comments, and Y. Murakami for technical assistance. One of the authors (T.S.) was supported by the Japan Society for the Promotion of Science for Young Scientists.

*go-sai@imr.tohoku.ac.jp

[1] J. C. Slonczewski, J. Magn. Magn. Mater. **159**, L1 (1996).
[2] L. Berger, Phys. Rev. B **54**, 9353 (1996).
[3] M. Tsoi, A. G. M. Jansen, J. Bass, W.-C. Chiang, M. Seck, V. Tsoi, and P. Wyder, Phys. Rev. Lett. **80**, 4281 (1998).
[4] E. B. Myers, D. C. Ralph, J. A. Katine, R. N. Louie, and R. A. Buhrman, Science **285**, 867 (1999).
[5] M. Tsoi, A. G. M. Jansen, J. Bass, W.-C. Chiang, V. Tsoi, and P. Wyder, Nature (London) **406**, 46 (2000).
[6] J. A. Katine, F. J. Albert, R. A. Buhrman, E. B. Myers, and D. C. Ralph, Phys. Rev. Lett. **84**, 3149 (2000).
[7] J. Grollier, V. Cros, A. Hamzic, J. M. George, H. Jaffrès, A. Fert, G. Faini, J. Ben Youssef, and H. Legall, Appl. Phys. Lett. **78**, 3663 (2001).
[8] S. Urazhdin, Norman O. Birge, W. P. Pratt, Jr., and J. Bass, Phys. Rev. Lett. **91**, 146803 (2003).
[9] S. I. Kiselev, J. C. Sankey, I. N. Krivorotov, N. C. Emley, R. J. Schoelkopf, R. A. Buhrman, and D. C. Ralph, Nature (London) **425**, 380 (2003).
[10] W. H. Rippard, M. R. Pufall, S. Kaka, S. E. Russek, and T. J. Silva, Phys. Rev. Lett. **92**, 027201 (2004).
[11] K. Yagami, A. A. Tulapurkar, A. Fukushima, and Y. Suzuki, Appl. Phys. Lett. **85**, 5634 (2004).
[12] G. D. Fuchs, N. C. Emley, I. N. Krivorotov, P. M. Braganca, E. M. Ryan, S. I. Kiselev, J. C. Sankey, D. C. Ralph, R. A. Buhrman, and J. A. Katine, Appl. Phys. Lett. **85**, 1205 (2004).
[13] Y. Huai, F. Albert, P. Nguyen, M. Pakala, and T. Valet, Appl. Phys. Lett. **84**, 3118 (2004).
[14] H. Kubota, A. Fukushima, Y. Ootani, S. Yuasa, K. Ando, H. Maehara, K. Tsunekawa, D. D. Djayaprawira, N. Watanabe, and Y. Suzuki, Jpn. J. Appl. Phys., Part 2 **44**, L1237 (2005).
[15] J. Hayakawa, S. Ikeda, Y. M. Lee, R. Sasaki, T. Meguro, F. Matsukura, H. Takahashi, and H. Ohno, Jpn. J. Appl. Phys., Part 2 **44**, L1267 (2005).
[16] S. Mangin, D. Ravelosona, J. A. Katine, M. J. Carey, B. D. Terris, and E. E. Fullerton, Nat. Mater. **5**, 210 (2006).
[17] T. Seki, S. Mitani, K. Yakushiji, and K. Takanashi, Appl. Phys. Lett. **88**, 172504 (2006).
[18] H. Meng and J.-P. Wang, Appl. Phys. Lett. **88**, 172506 (2006).
[19] D. Ravelosona, S. Mangin, Y. Lemaho, J. A. Katine, B. D. Terris, and E. E. Fullerton, Phys. Rev. Lett. **96**, 186604 (2006).
[20] T. Seki, S. Mitani, K. Yakushiji, and K. Takanashi, Appl. Phys. Lett. **89**, 172504 (2006).
[21] T. Seki, T. Shima, K. Yakushiji, K. Takanashi, G. Q. Li, and S. Ishio, J. Appl. Phys. **100**, 043915 (2006).
[22] E. B. Myers, F. J. Albert, J. C. Sankey, E. Bonet, R. A. Buhrman, and D. C. Ralph, Phys. Rev. Lett. **89**, 196801 (2002).
[23] R. H. Koch, J. A. Katine, and J. Z. Sun, Phys. Rev. Lett. **92**, 088302 (2004).
[24] Z. Li and S. Zhang, Phys. Rev. B **69**, 134416 (2004).
[25] T. Seki, S. Mitani, K. Yakushiji, and K. Takanashi, J. Appl. Phys. **99**, 08G521 (2006).
[26] J. Xiao, A. Zangwill, and M. D. Stiles, Phys. Rev. B **72**, 014446 (2005).
[27] J. Z. Sun, Phys. Rev. B **62**, 570 (2000).

[28] I. N. Krivorotov, N. C. Emley, J. C. Sankey, S. I. Kiselev, D. C. Ralph, and R. A. Buhrman, Science **307**, 228 (2005).
[29] K.-J. Lee, A. Deac, O. Redon, J.-P. Nozières, and B. Dieny, Nat. Mater. **3**, 877 (2004).
[30] Y. Acremann, J. P. Strachan, V. Chembrolu, S. D. Andrews, T. Tyliszczak, J. A. Katine, M. J. Carey, B. M. Clemens, H. C. Siegmann, and J. Stöhr, Phys. Rev. Lett. **96**, 217202 (2006).
[31] O. Ozatay, N. C. Emley, P. M. Braganca, A. F. G. Garcia, G. D. Fuchs, I. N. Krivorotov, R. A. Buhrman, and D. C. Ralph, Appl. Phys. Lett. **88**, 202502 (2006).
[32] X. Li, Z. Zhang, Q. Y. Jin, and Y. Liu, Appl. Phys. Lett. **92**, 122502 (2008).